Key Engineering Materials Vols. 523-524 (2012) pp 81-86
Online available since 2012/Nov/12 at www.scientific.net

doi:10.4028/www.scientific.net/KEM.523-524.81

Ultra-Precision Cutting of Single Crystal Silicon using Diamond Tool with Large Top Corner Radius

Yuya KOBARU[1,a], Eiji KONDO[1,b] and Ryuichi IWAMOTO[2,c]

[1]Kagoshima University, 1-21-40, Korimoto, Kagoshima 890-0065, JAPAN

[2]Kagoshima Prefecture Institute of Industrial Technology, 1445-1 Oda, Hayato-cho, Kirishima, 899-5105, JAPAN

[a]yu.yu.yu.0607@gmail.com, [b]kondo@mech.kagoshima-u.ac.jp, [c]iwamoto@kagoshima-it.go.jp

Keywords: Cutting Fluid, Large Top Corner Radius Tool, Single Crystal Silicon, Ultra-Precision Cutting

Abstract. A lot of studies on the ultra-precision cutting of single crystal silicon have been reported and they used the single crystal diamond cutting tools having the sharp cutting edge. However, the diamond cutting tools having small chamfer at the cutting edge are usually used in practical machining shops. In addition, studies on the relationship between the tool wear and the machined surface have been reported little although the relationship is important in practical applications. In this study, ultra-precision cutting of single crystal silicon, using cutting fluids, feed rate, and depth of cut as experimental parameters, was carried out with the single crystal diamond cutting tools having small chamfer and large nose radius, and the effects of the experimental parameters on the machining accuracy and tool wear were investigated. As a result, the optimum cutting conditions was obtained as follows: the cutting fluid was kerosene, the feed rate was 2.0μm/rev, and the depth of cut was 1.0μm.

1. Introduction

The single crystal silicon is used as materials of the infrared lenses because the silicon has high transmissivity and refractive index to the wavelength of an infrared domain. The single crystal silicon lenses are usually fabricated by combining the grinding process with the polishing process because the silicon material has a high melting point while the general glass lenses are usually fabricated by molding [1,2]. However, it has been attempted to fabricate the single crystal silicon lenses by cutting because it is difficult for conventional grinding and polishing processes to perform the aspherical lenses and make the accurate shape of the lens. A lot of studies on the ultra-precision cutting of single crystal silicon have been reported. For example, it has been reported that the ductile-brittle transition point can be evaluated uniquely in the critical uncut chip thickness in cutting process with a single crystal diamond tool having straight nose [3], and the critical uncut chip thickness is alternated by the rake angle [4]. However, it is difficult to apply the cutting tools having straight nose to machining the concave lenses because the cutting tools interfere with the concave machined surface of the lens [5]. Therefore, the single crystal diamond tools having large nose radius have to be used to fabricate the concave lenses. It has been reported in the study on machining the single crystal silicon materials with the single diamond cutting tools having large nose radius that the conditions of ductile-brittle transition could be evaluated from the cracks caused by the indentation tests [6]. However, in the previous studies as mentioned above, the cutting tools having the sharp cutting edge are used on cutting tests although the diamond cutting tools having small chamfer at cutting edge are usually used in practical machining shops. In addition, relationship between the tool wear and the machined surface is important in practical applications but studies on the relationship have been reported little.

In this study, ultra-precision cutting of single crystal silicon, using cutting fluids, feed rate, and depth of cut as experimental parameters, were carried out with the single crystal diamond cutting tools having small chamfer at cutting edge and large nose radius, and the effects of the cutting fluids, the feed rate, and the depth of cut on the machining accuracy and tool wear were investigated.

2. Experimental Apparatus and Methods

Single crystal diamond cutting tools used in this study had the large nose radius and the small chamfer at the cutting edge shown in Fig. 1 [7]. Cutting tests were carried out on the ultra-precision lathe (Toyoda Machine Works: AHN60-3D). Experimental conditions are shown in Table 1. In the cutting tests, the tool was fed from the outside of the workpiece to its center to machine the workpiece surface. Cutting forces were measured by the dynamometer (Kistler: 9246A) installed on the tool holder. The surface of the workpiece of more than 32 mm radius and less than 8 mm in radius was removed in advance for cutting tests as shown in Fig. 2 in order to prevent the unpredictable chipping of the cutting edge. Properties of the cutting fluids made of the plant oil and the kerosene used as the cutting fluid are shown in Table 2. The wear of the cutting edge was observed by the SEM (scanning electron microscope). The shape of the machined surface was measured by the form measuring instrument. The roughness of the machined surface was measured by the interferometer (ZYGO: New View 5032).

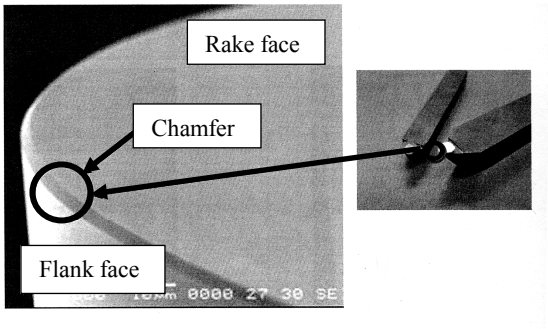

Fig.1 Photograph of new cutting tool

Table1 Experimental conditions

Workpiece	Material	Single crystal Silicon (100)	
	Diameter [mm]	76.2	
	Thickness [mm]	6	
Tool	Material	Single crystal diamond	
	Nose radius [mm]	2	
	Rake angle [deg.]	0	
	Clearance angle [deg.]	4	
	Chamfer [μm]	2 (-45deg)	
Spindle speed [rpm]		1000	
Depth of cut d [μm]		1.0	0.5, 1.0, 1.5
Feed rate f [μm/rev]		0.5, 1.0	0.5~8.0
Cutting fluid		Plant oil	Kerosene

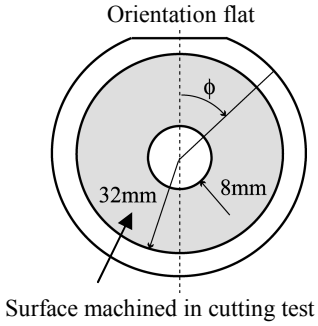

Fig.2 Workpiece

Table2 Properties of cutting fluids

	Plant oil	Kerosene
Density [g/cm^3]	0.92	0.80
Kinematic viscosity [mm^2/s]	41.80	2.78
Surface tension [mN/m]	32.82	27.68

3. Results and Considerations

3.1 Effects of cutting fluids

Figure 3 shows the photographs of the cutting edge when the feed rate is 0.5μm/rev and the depth of cut is 1.0μm. The chipping of the cutting edge is observed as shown in Fig. 3 (a) when the plant oil cutting fluid is used. On the other hand, when the kerosene is used as the cutting fluid, the chipping does not occur although the flank wear of the cutting edge is observed. Figure 4 shows the principal forces and Figure 5 shows the thrust forces in the early stage of the machining when the feed rates are 0.5 and 1.0μm/rev. It can be seen from Figs. 4 and 5 that the principal force and the thrust force are larger with the plant oil cutting fluid than with the kerosene, respectively. When the rake angle is expressed by α and the friction angle is by β, the angle (β - α) can be calculated from the cutting forces shown in Figs. 4 and 5 by Eq. (1).

$$\beta - \alpha = \tan^{-1}\left(F_z / F_y\right). \tag{1}$$

The calculated angles (β - α) are shown in Fig. 6 and they demonstrate that the friction angle on rake face β with the plant oil cutting fluid is larger than the friction angle β with the kerosene since the rake angle α is expected to be constant at each feed rate. Furthermore, it can be considered from Table 2 that the larger kinematic viscosity of the plant oil cutting fluid resulted in the larger friction angle shown in Fig. 6.

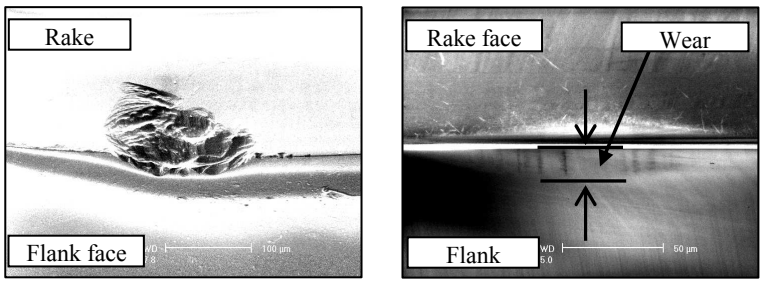

(a) Plant oil (b) Kerosene

Fig.3 Photographs of cutting edge

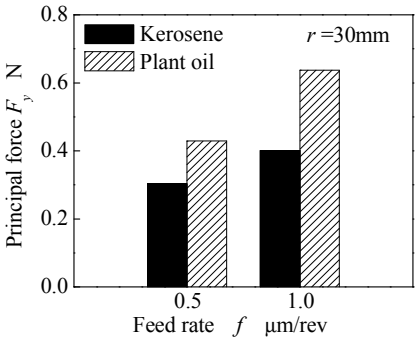

Fig.4 Principal force

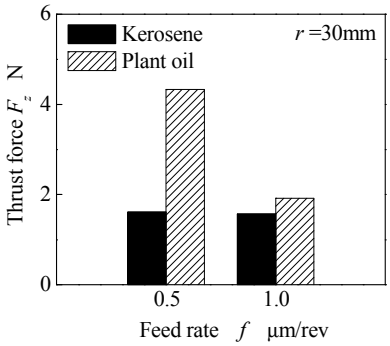

Fig.5 Thrust force

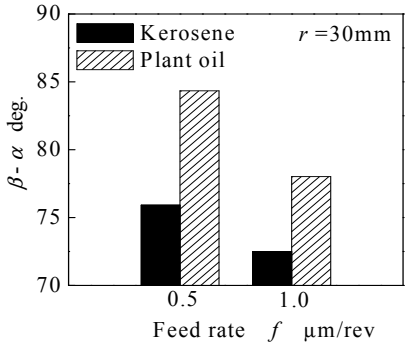

Fig.6 The apparant friction angle (β - α)

3.2 Effects of feed rate and depth of cut

3.2.1 Surface roughness

After this, all experimental results will be obtained by the cutting tests with the kerosene. The photographs of the machined surfaces are shown in Fig. 7 at the feed rates of 0.5, 2.0, and 8.0μm/rev, respectively. When the feed rate is 2.0μm/rev, the machined surface is glossary and it reflects the lattice pattern. When the feed rate is 0.5μm/rev, the machined surface is pear skin. When the feed rate is 8.0μm/rev, the machined surface is a little glossy. Figure 8 shows the detail of machined surface observed by the interferometer in case of the feed rate of 2.0μm/rev where the machined surface is glossy. The cutter marks with each space of the feed rate can be observed in Fig. 8. Figure 9 shows the roughness of the surface as shown in Fig. 8. The surface roughness decreases with increase of the feed rate by 2.0μm/rev, and then it increases over 2.0μm/rev. Consequently, the surface roughness is the minimum at the feed rate of 2.0μm/rev, where is about 6nm. It can also be seen in Fig. 9 that the surface roughness becomes larger when the depth of cut is larger and smaller than 1.0μm.

Figure 10 shows the relationship between the thrust forces F_z and the distance from the center of the workpiece L at the depth of cut of 1.0μm. It can be seen in Fig. 10 that the thrust forces are almost constant when the larger feed rates are from 2.0 to 8.0μm/rev but they increases with decrease of the distance from the center at smaller feed rates of 0.5 and 1.0μm/rev. Figure 11 shows the thrust forces with increase of the cutting distance. It can be seen in Fig. 11 that the thrust forces keep constant by the cutting distance of about 1.25km. Therefore, it can be considered that the effect of tool wear on the cutting forces is little when the cutting distance is less than 1.25km. Figure 12 shows the average of the cutting forces within the cutting distance of 1.25km. The average thrust force F_z monotonously decreases with increase of the feed rate while the principal force F_y increases by 2.0μm/rev and then decreases over 2.0μm/rev. The thrust and principal forces hardly change even if the depth of cut is larger and smaller than 1.0μm.

Figure 13 shows the cutting cross section ABC where the uncut chip thickness increases from 0 to h_{max}. The maximum uncut chip thickness h_{max} can be calculated by the Eq. (2) where f is the feed rate, d is the depth of cut, and R is the nose radius of the cutting tool top.

$$h_{\max} = f\sqrt{(2d/R)+(d/R)^2}\ . \tag{2}$$

The mean uncut chip thickness h_{mean} is the half of the maximum uncut chip thickness $h_{\max}$. Figure 14 shows the angle (β-α), which is calculated by Eq. (1), with increase of the mean uncut chip thickness h_{mean}. The obtained angle (β-α) decreases at smaller uncut chip thickness and it reaches the minimum at the thickness of 0.03μm where the angle (β-α) is about 68 degrees. As the friction angle β is expected to be almost constant in this case, it can be considered that the decrease of the angle (β-α) at the thickness of less than 0.03μm is caused by the cutting edge roundness. According to previous study, the critical uncut chip thickness decreased with decrease of the rake angle less than -40 degrees [4]. In addition, the critical uncut chipthickness is about 0.01~0.03μm for the machining of single crystal silicon material by the single crystal diamond tool having large nose radius [8]. Therefore, it is considered that the pear skin of the machined surface at the feed rate of less than 2.0μm/rev is caused by the decrease of the effective rake angle where the uncut chip thickness is less than the radius of the cutting edge roundness.

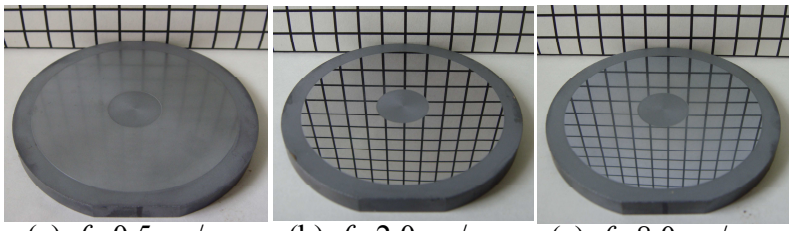

(a) f=0.5μm/rev (b) f=2.0μm/rev (c) f=8.0μm/rev

Fig.7 Photographs of machined surface

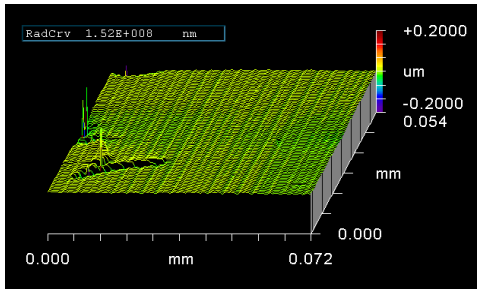

Fig.8 Detail of machined surface (f=2.0μm/rev, d=1.0μm)

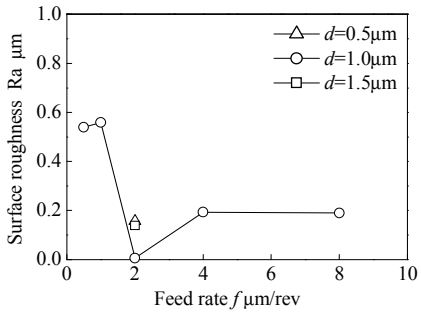

Fig.9 Surface roughness

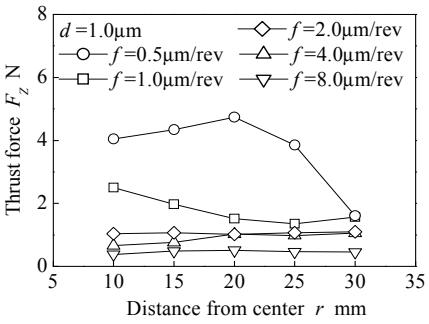

Fig.10 Relationship between thrust force and distance from center

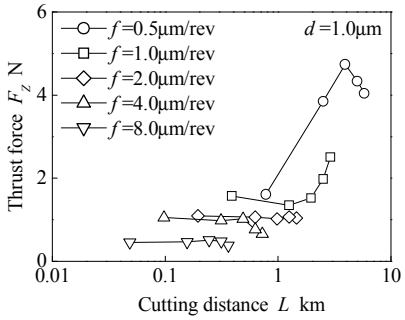

Fig.11 Relationship between thrust force and cutting distance

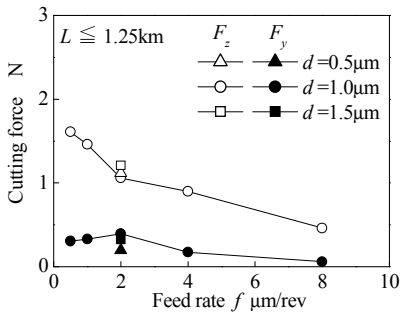

Fig. 12 Cutting forces

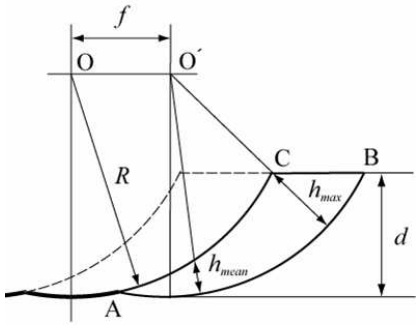

Fig. 13 Cutting geometry viewed in the direction normal to cutting direction

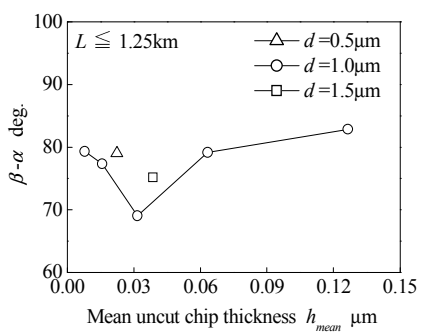

Fig. 14 Relationship between (β- α) and mean uncut chip thickness

3.2.2 Tool wear

Figure 15 shows the width of flank wear land as shown in Fig. 3(b). The measured width of flank wear land rapidly decreases by the feed rate of 2.0μm/rev with increase of the feed rate and then it gradually decreases. Figure 16 shows the width of flank wear land with increase of the cutting distance and the wear increases at almost constant wear rate which is about 3.0μm/km. Figure 17 shows the mean thrust forces which are average of the thrust forces F_z shown in Fig. 10, respectively. The average principal forces F_y are calculated in the same way as the average thrust forces. The average thrust force decreases with increase of the feed rate, which is similar to the width of flank wear land shown in Fig. 15. Figure 18 shows the relationship between the average thrust force and the width of flank wear land. It can be seen in Fig. 18 that the average thrust force is approximately proportional to the width of flank wear land.

3.2.3 Flatness

Figure 19 shows the shape of the machined surface when the feed rate is 0.5μm/rev. It can be seen in Fig. 19 that the machined surface is convex. Figure 20 shows the flatness of machined surface with increase of the feed rate. The flatness is defined as average of the maximum heights in three directions at angle of 0, 45, 90 degrees shown in Fig. 19. The flatness decreases with increase of the feed rate, which is similar to the width of flank wear land shown in Fig. 15. As the workpiece is machined with the cutting tool fed from the outside to the center of the workpiece, it can be considered that the convex surface is generated by the tool flank wear. The conceptual figure of worn cutting edge is illustrated in Fig. 21 where the width of flank wear land V_B can be related to the recession of cutting edge δ. Furthermore, the recession δ can be calculated from the width V_B by Eq. (3).

$$\delta = V_B / (\cot\gamma + \tan\alpha) \tag{3}$$

where γ is the clearance angle and α is the rake angle. The measured flatness related to the width of flank wear land is represented by the open marks in Fig. 22. The solid line in Fig. 22 denotes the theoretical flatness calculated by Eq. (3) on the assumption that the flatness equals the recession δ

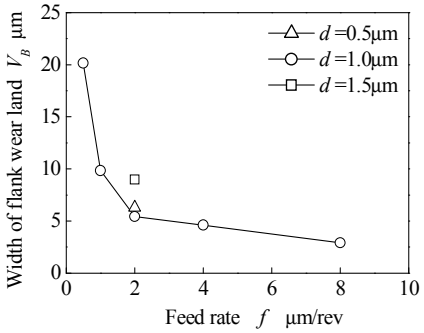

Fig. 15 Width of flank wear land

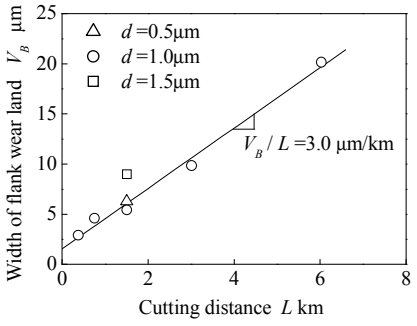

Fig. 16 Relationship between width of flank wear land and cutting distance

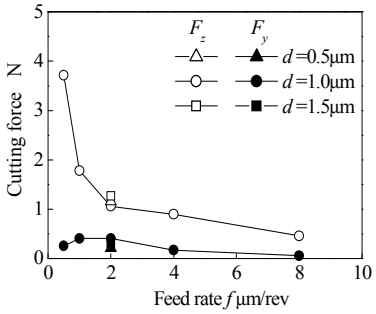

Fig. 17 Mean value of cutting force

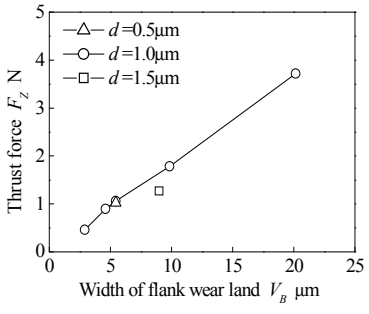

Fig. 18 Relationship between thrust force and width of flank wear land

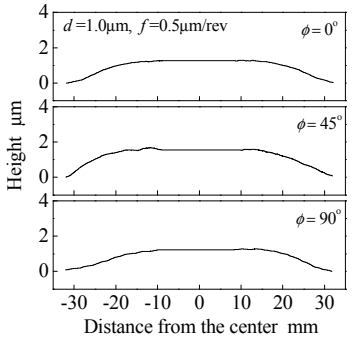

Fig. 19 Shape of machined surface

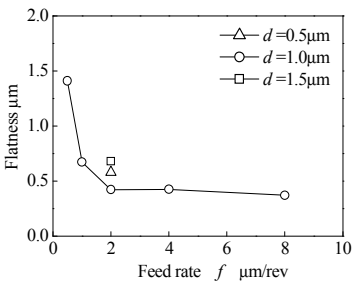

Fig. 20 Flatness of machined surface

shown in Fig. 21. It can be seen that the measured flatness approximately coincide with the theoretical flatness. Consequently, it is considered that the flatness of the machined surface is strongly affected by the tool flank wear.

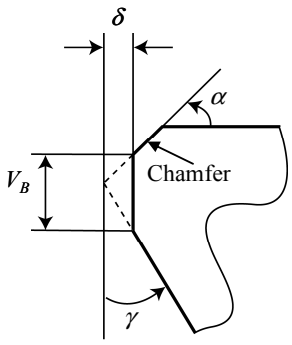

Fig. 21 Conceptual figure of worn cutting edge

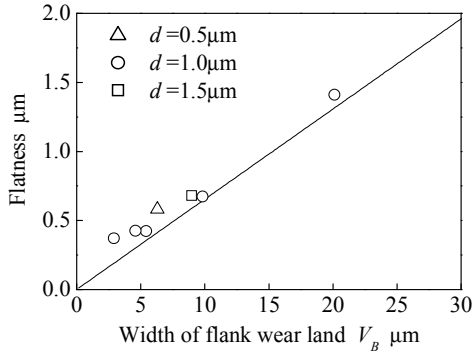

Fig. 22 Relationship between flatness and width of flank wear land

4. Conclusion

(1) The chipping of the cutting edge occured when the cutting fluid made of the plant oil was used but there was no cutting edge chipping with the kerosene used as the cutting fluid.
(2) The machined surface was glossy when the cutting fluid was the kerosene, the depth of cut was 1.0 μm, and the feed rate was 2.0μm/rev, but the machined surface was pear skin under other cutting conditions even if the depth of cut was smaller than 1.0μm or the feed rate was smaller than 2.0μm/rev.
(3) Effect of the tool wear on the cutting forces could be neglected by the cutting distance of 1.25km.
(4) When the friction angle on rake face was expressed by β and the rake angle was α, (β -α) was minimum at feed rate of 2.0μm/rev where the mean uncut chip thickness was about 0.03μm.
(5) The tool flank wear rate (increment of width of flank wear land per unit cutting distance) was about 3.0μm/km and the wear rate was hardly affected by the feed rate and the depth of cut.
(6) The thrust force linearly increased with increase of the width of flank wear land.
(7) The flatness of the machined surface approximately coincided with the recession length of the cutting point estimated from the width of flank wear land by the geometrical calculation.

References

[1] H. Huang, BL. Wang, Y. Wang, J. Zou and L. Zhou. Materials Science and Engneering A. 479, 1-2 (2008) 373-379
[2] W.K. Chen, T. Kuriyagawa, H. Huang and N. Yosihara. Journal of the International Societies for Precision Engineering. 29, 3 (2005) 315-323
[3] J. Yan, K. Syoji, H. Suzuki and T. Kuriyagawa. Japan Society for Precision Engineering. 64, 9 (1998) 1345-1349 (in Japanese)
[4] J. Yan, K. Syoji and T. Kuriyagawa. Japan Society for Precision Engineering. 66, 7 (2000) 1130-1134 (in Japanese)
[5] T. Ota, J. Yan, S. Kodera, S.Yajima, Y. Takahashi, N. Horikawa and T. Kuriyagawa. Japan Society for Abrasive Technology. 52, 11 (2008) 651-656 (in Japanese)
[6] T. Shibata, S. Fujii, A. Fujii, E. Makino and M. Ikeda. Japan Society for Precision Engineering. 62, 11 (1996) 1632-1637 (in Japanese)
[7] Information on http://www.allied-material.co.jp/products/diamond/cutting/upc2/
[8] Y. Ichida, N. B. Frej and R. Yousefi. Japan Society for Precision Engineering. 64, 4 (1998) 608-612 (in Japanese)

Emerging Technology in Precision Engineering XIV
10.4028/www.scientific.net/KEM.523-524

Ultra-Precision Cutting of Single Crystal Silicon Using Diamond Tool with Large Top Corner Radius

10.4028/www.scientific.net/KEM.523-524.81